ELSEVIER

Nuclear Instruments and Methods in Physics Research A 484 (2002) 299–311

NUCLEAR INSTRUMENTS & METHODS IN PHYSICS RESEARCH Section A

www.elsevier.com/locate/nima

High-sensitivity, portable, tunable imaging X-ray spectrometer based on a spherical crystal and MCP

P. Monot[a], T. Auguste[a], S. Dobosz[a,*], P. D'Oliveira[a], S. Hulin[a], M. Bougeard[a], A.Ya. Faenov[b], T.A. Pikuz[b], I.Yu. Skobelev[b]

[a] *CEA, Centre D'Etudes de Saclay, DSM/DRECAM, Service des Photons Atomes et Molécules, Ba.524, F-91191 Gif-sur-Yvette, Cedex, France*

[b] *Multicharged Ions Spectra Data Center of VNIIFTRI, Mendeleevo, Moscow region 141570, Russia*

Received 2 April 2001; accepted 11 September 2001

Abstract

A portable ($200 \times 100 \times 100\,mm^3$), high-luminosity, spherically bent crystal spectrometer was designed to measure very low emissivity X-ray spectra of different elements with spatial resolution in a wide spectral range (1.2–19.6 Å). A large ($50 \times 15\,mm^2$) open aperture mica spherically bent crystal with $R = 150\,mm$ was used as dispersive and focusing element. This spectrometer was associated with a large sensitive area ($\phi = 40\,mm$) micro-channel plates assembly. This apparatus provides simultaneously high spectral ($\lambda/\delta\lambda \sim 1800$) and spatial (100–200 μm) resolutions. Its large tunability allowed, without any adjustment of the spectrometer set-up, to record spectra in the 1.38–17.5 Å wavelength range. We used the X-ray emission of femtosecond laser-produced plasmas from different materials ($(CF_2)_n$, CaF_2, Cu, Al) to test the spectrometer. Thanks to the high sensitivity (high collection efficiency) of the system, high quality space-resolved X-ray spectra of Fluorine and Aluminum plasmas were obtained on a single laser shot.

PACS: 7.85.Nc; 32.30.Rj; 52.70.La

Keywords: X-ray spectrometer; Plasma; Spatial and spectral resolutions; Micro-channel plates (MCP)

1. Introduction

The X-ray spectroscopy of atoms and ions covers nowadays a wide range of fields in physics, extending from the atomic physics to the study of matter irradiated by high-intensity lasers [1–4]. X-ray emission is typically measured whether with good spatial, but poor spectral resolution (for example, typical X-ray charge coupled device (CCD) has spatial resolution about 10–20 μm and energy resolution about 300 eV), or good spectral resolution (different types of crystal spectrometers are used), but without spatial resolution. However, many investigations require to collect simultaneously informations about spatial and spectral distributions of X-ray emission with good resolution.

*Corresponding author. Tel.: +33-1-69-086340; fax: +33-1-69-088707.

E-mail address: dobosz@drecam.cea.fr (S. Dobosz).

0168-9002/01/$ - see front matter
PII: S0168-9002(01)01991-X

Such problem can usually be solved by placing a slit in the direction perpendicular to the spectral dispersion of the crystal. Unfortunately, the quality of spectroscopic measurements is generally not very high due to the weak intensity of the lines emission and the poor luminosity of flat crystal spectrometers commonly used in such studies. Additionally, placing a slit decreases the throughput of the spectrometer. The detection efficiency of X-ray spectrometers can be increased by using cylindrically bent crystals as dispersive elements. However, it is still necessary to put a slit to achieve a good spatial resolution of X-ray emission.

Recently, new types of bent crystal spectrometers—Focusing Spectrometers with Spatial 1D and 2D Resolution (FSSR-1, 2D spectrometers), based on spherically bent crystals with a large open aperture and small radius of curvature started to be used [5–8]. The advantage of this apparatus is the absence of slit, while providing both spectral and spatial resolutions. High spectral and spatial resolutions as well as high luminosity are achieved in FSSR-1, 2D spectrometers by using the focusing properties of spherically bent crystals. In most experiments, these spectrometers were used in conjunction with photographic films as a detector. This prevented from receiving real time information during the experimental run.

Fortunately, significant progresses were completed by the development of thinned-back illuminated CCD camera, sensitive in the X-ray domain. The advantages of combining a FSSR-1, 2D spectrometer with such a X-ray CCD camera were successfully demonstrated in high-resolution X-ray spectromicroscopy experiments performed on the Tokyo electron beam ion trap X-ray source [9]. However, in order to obtain a reasonable dynamics (16 bits), these devices have to be cooled, and the repetition rate of acquisition is restricted to approximately $1\,s^{-1}$ to limit the readout noise. This repetition rate is well below the one of many experiments involving X-ray detection. Moreover, they offer a small field of view (a few cm^2) and electronic as well as mechanical shutters avoid any gated operation below the ms range. Their sensitivity to visible and near infrared light strongly limits their applications in the field of laser–matter interaction. Finally, the cost of such devices limits considerably their use in laboratories. On the other hand there exists even more luminous X-ray spatially resolving detectors—micro-channel plates (MCP). These X-ray detectors are cheaper and have a larger field than X-ray cameras.

In this paper we present details of the construction and the first results obtained with a portable, tunable, high-sensitive X-ray spectrometer based on a spherically bent mica crystal and a MCP assembly. The combination of FSSR-1, 2D spectrometers with a MCP assembly increases the luminosity and flexibility of such spectrometers and allows to record new informations on femtosecond laser interaction with a wide variety of solid targets, with a high repetition rate (20 Hz), allowing for gated operation in the nanosecond range, and for a moderate cost.

2. Spectrometer configuration

2.1. The geometry of a spherically curved crystal X-ray spectrometer

The FSSR-1, 2D spectrometers, based on spherically bent crystals, utilize both the focusing aspects of the spherical mirror configuration as well as the Bragg crystal X-ray diffraction. They allow to receive spectrally resolved images of X-ray sources simultaneously with spatial resolution. The main properties of such spectrometers can be explained using two independent mutually perpendicular planes: the dispersion plane and the sagittal or focusing plane. Since the spherical crystal itself has indeed no specific geometrically determined plane, the first one can be defined by the position of the source, the detector and the crystal pole (Y orientation). The second one is just perpendicular to the first one (X orientation) (see Fig. 1).

In the dispersion plane, the source beam reflection from the crystal is related to the Bragg condition

$$2d_n \sin \Theta = n\lambda \tag{1}$$

where λ is the wavelength, Θ is the glancing angle, n is the order of diffraction; d_n is the interplanar

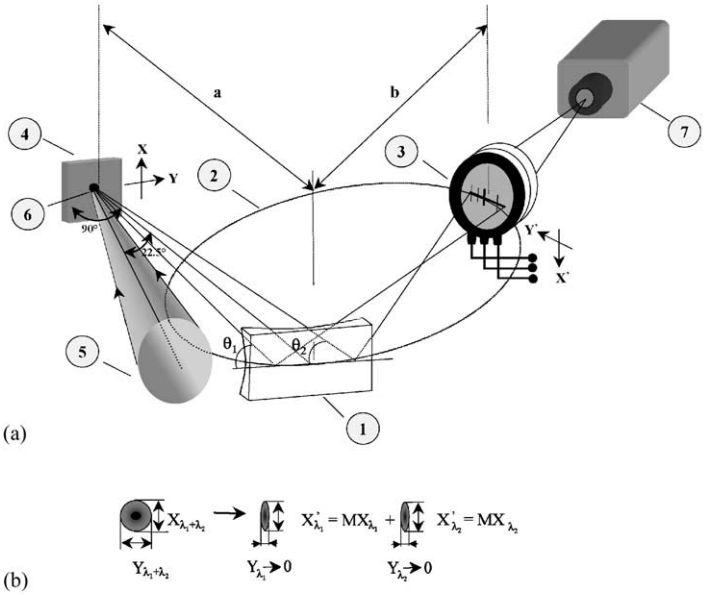

Fig. 1. (a) Optical scheme for the formation of X-ray spectra in a FSSR-1D spectrometer: (1) spherically bent crystal, (2) Rowland circle, (3) MCP assembly, (4) solid target, (5) laser beam, (6) laser-produced plasma X-ray source, (7) video camera for transformation of spectral image from MCP to the computer. a—Distance between the X-ray source and the spherical crystal, b—distance between the spherical crystal and the MCP assembly. (b) Schematic representation for the transformation of a polychromatic X-ray plasma source radiation to one-dimensional spatially resolved monochromatic image on the detector surface.

distance for the nth diffraction order. After reflection from the crystal, spectrally selected X-ray beams are formed in this plane.

In the saggital plane, due to the focusing properties of spherical crystal surfaces, such reflected beams create spectrally resolved images of the source. The position of the best focus as well as the best spatial resolution are given by the usual equation [7]:

$$1/a + 1/b = (2\sin\Theta)/R \tag{2}$$

where a is the distance from the source to the crystal pole, b is the distance from the crystal pole to the image plane, and R is the crystal radius of curvature. At the position b the images have a linear magnification $M = b/a$.

In the case of the FSSR-1D spectrometer the X-ray detector is placed on the Rowland circle in order to obtain a spectral resolution independent of the X-ray source size (by analogy with a classical Johann spectrometer where a cylindrically bent crystal is used). Thus, the distance from the crystal pole to the detector is $b = R\sin\Theta$. It follows that, in order to obtain the best spatial resolution on the detector in the saggital plane, the source has to be set up at the distance a from the crystal (according to Eq. (2)), such as

$$a = R\sin\Theta/(2\sin^2\Theta - 1). \tag{3}$$

As a result, in the detector plane, spectrally resolved images of the X-ray source are formed. It means that the original source, which emits different wavelengths, is observed as a set of monochromatic 1D images. The size of these images is spatially transformed from the original source shape (see Fig. 1a): the X' size of the images in the saggital direction is changed by a linear magnification: $X' = MX$, where $M = -\cos 2\Theta$. In the plane of dispersion, the Y' size of the images does not depend on the size of the source and depends only on the spectral line width and on the width of the crystal reflection curve.

In the case of the FSSR-2D spectrometer, the detector can be placed in any position compared to

the Rowland circle, but Eq. (2) must still be satisfied. For example, if distance $a = R\sin\Theta$ (now the source is on the Rowland circle), then

$$b = R\sin\Theta/(2\sin^2\Theta - 1). \quad (4)$$

In such a scheme, the linear magnification in the saggital plane is given by $M = -1/\cos 2\Theta$. In the tangential plane (dispersion plane), the size of the image depends on the size of the source. A large source size drastically reduces the spectral resolution. A detailed study on the dependency of the spectral resolution with the source size is presented in Ref. [8] for different distances and angles. In order to optimize FSSR-1D or FSSR-2D spectrometer parameters for specific experimental conditions and to get a fast estimation of its spectral resolution, a dedicated software package has been developed in MISDC of VNIIFTRI [10].

2.2. MCP assembly

The MCP assembly is composed of a pair of 42 mm-diameter, 480 μm-thickness array of microcapillaries. Secondary electrons outgoing from the 12 μm-diameter channels are accelerated towards a phosphor screen whose emission is centered at 545 nm. A mirror reflects the emission out of the experimental chamber through a glass window. A single-shot non-interlaced CCD camera equipped with a standard objective images the phosphor screen. Due to the $\frac{1}{6}$ magnification, each pixel corresponds to a size of 60 μm (vertical) × 50 μm (horizontal) in the phosphor screen plane. The CCD exposure and readout are synchronized to the laser shots. An iris allows to adapt the input signal to the camera sensitivity. The video signal is sent towards a frame grabber that digitizes the image over 8 bits. The power supplies that deliver high voltage to MCP and phosphor screen are linked to the computer via a GPIB interface. In order to limit the signal fluctuations due to variations of the applied potentials, high precision-regulated power supplies were chosen. They have an accuracy of 0.05% and exhibit ripples less than 0.0015%. For each laser shot, one records the MCP phosphor screen image, the applied high voltages and the laser energy. The spatial resolution of 100 μm is limited by the large channel diameter. It will soon be lowered to 25 μm by the use of a 6 μm channel diameter assembly.

The large number of secondary emission following the ejection of one single primary electron compensates the relatively poor quantum efficiency (10%) [11] of MCP in the soft X-ray domain. Furthermore, a very large differential dynamics is obtained by varying the high voltage applied to MCP. Fig. 2 shows the relative evolution of the gain factor as a function of the applied voltage deduced from our experimental measurements compared with the theoretical curve given by the MCP manufacturer (Hamamatsu). For the sake of comparison, experimental data were normalized to the theoretical ones for a voltage of 1.2 kV. A MCP dynamics of 300 is obtained by varying the voltage from 1 to 1.5 kV. The potential was limited to 1.5 kV in order to prevent electrical breakdown whereas the manufacturer specification indicates that 2 kV can be applied. This dynamics is increased by a factor of 256 due to the 8 bit camera ADC. The camera objective includes an iris, which allows to vary the input signal on the CCD by more than a factor of 100. The full range

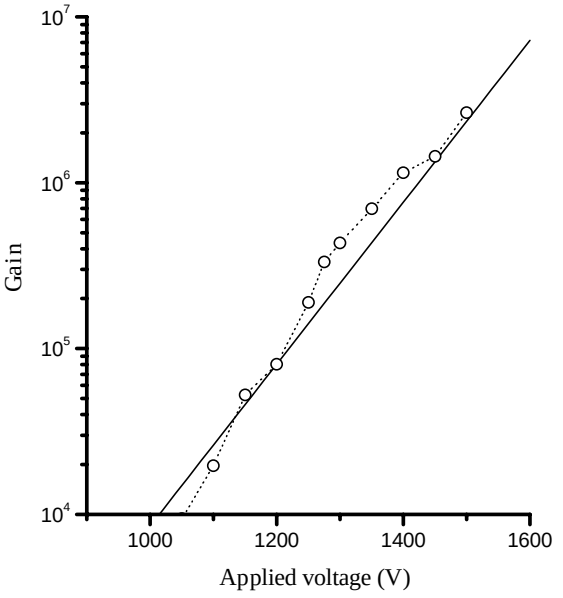

Fig. 2. Gain factor of the MCP assembly as a function of the voltage applied on it—experimental points (open circles), typical curve given by the manufacturer (solid line).

of the signal then exceeds 10^6. This dynamics is much larger than the one obtained using thinned-back illuminated 16 bits X-ray CCD cameras.

2.3. Spectrometer set-up.

Large open aperture spherically bent crystals of mica with different radii of curvature $R = 100$, 150, 250 mm and differently oriented quartz crystals are produced routinely now at the MISDC of VNIIFTRI (Russia). The choice of a crystal for a given experiment results from a compromise between luminosity and spectral resolution. On the one hand, for the purposes of the present experiment (registration of weak X-ray spectra) it was necessary to increase the spectrometer luminosity. In such case the distance between the crystal and the plasma must be as small as possible and it is necessary to choose spherically bent mica crystals with minimum radius of curvature. On the other hand, the spectral resolution is an increasing function of the radius of curvature. As a compromise in front of this contradicted situations, a crystal with $R = 150$ mm was chosen as a spectrometer dispersive element. The linear sizes of the crystal are $50 \times 15\,\mathrm{mm}^2$.

An interesting property of mica crystals relies on their very good reflectivity in the different diffraction orders. Practically, it is possible to observe spectra in I, II, III, IV, V, VII, VIII, XI, XII and XIII diffraction orders. As the lattice space of mica crystal in the first order of diffraction is $2d \approx 19.91$ Å, it becomes possible to cover a very wide spectral range from about 1.2 up to 19 Å and thus to measure X-ray spectra from targets with very different nuclear charges Z.

The tunability of the spectrometer requires 5 degrees of freedom (3 rotations-2 translations). Special mini spectrometers were constructed for this purpose. Such a mini spectrometer includes the spectrometer body (see scheme in Fig. 3), on which were mounted the spherical crystal (1), 3 mini goniometers (4) and the MCP assembly (2). Mini goniometers are necessary for precise alignment of FSSR-1, 2D spectrometers according to ray-tracing calculations [10]. To cover a wider spectral range, it is possible to move the MCP (2) on the spectrometer body according to FSSR-1, 2D alignment requirements. We would like to underline that the overall size of the presented spectrometer is very small and does not exceed $200 \times 100 \times 100\,\mathrm{mm}^3$.

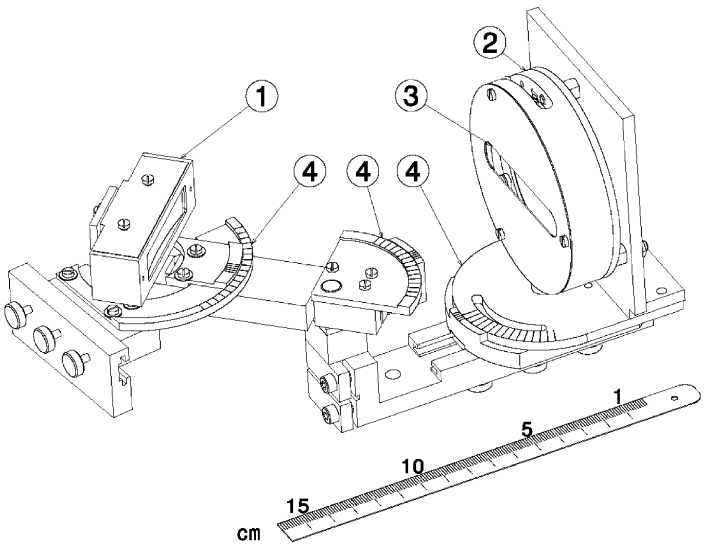

Fig. 3. (a) Schematic design of a spherical spectrometer with an MCP detector: 1—box with a spherically bent crystal, 2—holder with MCP, 3—1 μm polypropylene foil for MCP protection from VUV radiation, 4—mini goniometers.

Alignment of the FSSR-1, 2D spectrometers unfolds in 3 stages. First, the angles and distances on the spectrometer body are set up out of the vacuum chamber according to the data obtained from software calculations. Then, the whole spectrometer body with aligned crystal and MCP is placed inside the vacuum chamber such that the distance between the crystal and the target corresponds to the calculated preliminary distance [10]. Finally, the quality of the total alignment is checked with a He–Ne laser. The spectrometer allows to use Bragg angles between 30° and 75°. This means that, using different diffraction orders of the mica crystal, it is possible to measure spectra in a very wide spectral range, from 1.2 to 19.6 Å.

The total spectral resolution of the spectrometer is given by the following conditions:

(1) The intrinsic spectral resolution of the crystal is due essentially to imperfections in the crystalline lattice. It is well known that mica is not a perfect crystal, but as it was shown experimentally and theoretically in Refs. [12,13] the spectral resolution $\lambda/\delta\lambda$ can reach values higher than 1000 for wavelengths around 19 Å and about 10 000 for wavelengths smaller than 10 Å. It was also demonstrated that the spectral resolution does not decrease even with very short radii $R = 100$, 150 mm, provided that the spherical bending of the crystal is precise.
(2) The spectral resolution $\lambda/\delta\lambda$ given by the detector spatial resolution dx. In this case $\lambda/\partial\lambda = \lambda/((d\lambda/dx)\times dx)$ where $d\lambda/dx$ is the spectral dispersion. The ratio $\lambda/(d\lambda/dx)$ is equal for the whole spectral range covered in the present experiment (1.5–17 Å). Consequently, the 100 μm spatial resolution of MCP assembly leads to resolution $\lambda/\delta\lambda \geqslant 1800$.
(3) The spectral resolution given by the size of the X-ray source. As it was demonstrated in Ref. [14], the spectral resolution in the case of a detector located on the Rowland circle (FSSR-1D) is not limited by the source size. In this article, we have also considered the possibility of placing the detector out of the Rowland circle. It was demonstrated that even in such a case, spectral resolution $\lambda/\delta\lambda \approx 5000$ can be achieved for typical sizes of laser-produced plasma X-ray source, around 50–500 μm.

Thus, on the whole wavelength range considered here (1.2–19 Å), the spectral resolution of our spectrometer is limited by the detector spatial resolution and achieves $\lambda/\delta\lambda \approx 1800$.

In order to demonstrate the performances of the FSSR-1, 2D spectrometers associated to the MCP, several test experiments were conducted, recording the X-ray emission of femtosecond laser-produced plasmas using different Z materials.

3. The femtosecond laser facility and the experimental set-up

The experiments reported here were carried out on the 10 TW laser facility (UHI-10) at Saclay Laboratory (CEA, France). Such a laser system was designed to generate 60-fs pulses at 10 Hz. It employs the standard Chirped-Pulse-Amplification (CPA) technique. Ti-Sapphire rods are used as laser medium and the operating wavelength of the system is 790 nm. In order to produce such high-power ultrashort pulses with a good contrast, firstly, the low energy ultrashort pulse (linear p-polarized) is stretched up to 300 ps by an aberration free Offner stretcher, and secondly, it is amplified. The pulse energy is about 1.8 J after four stages of amplification. Then the compression is performed in a vacuum chamber directly connected to the experimental chamber. The contrast, measured with a high dynamics cross-correlator is about 10^{-5} at 1 ps, and about 10^{-7} at several ns. The post- and pre-pulses amplitudes are less than 10^{-5}. Total energy in the laser pulse was up to 800 mJ. The 80 mm diameter laser beam was focused with an $f/2.35$ off-axis parabolic mirror onto various solid targets as teflon $(CF_2)_n$, Al, CaF_2, and Cu slabs which were placed at 22.5° to the direction of the incident laser. The $1/e^2$ focal spot radius measured in vacuum was about 20 μm, giving a laser intensity on the target up to 10^{18} W/cm^2.

The diagnostic set-up is shown in Fig. 1. The $R = 150$ mm crystal (1) was placed at a distance of

350 mm from the plasma (6) and the sensitive plane of the MCP assembly (3) was located on the Rowland circle (FSSR-1D configuration).

The spectrometer has been placed (Fig. 1) normal to the target surface (4) and oriented in such a way that the spatial resolution was along the X direction, i.e., perpendicular to the plasma expansion. The magnification on the MCP surface was about $M = 1/2.8$ *. Then the 100 μm spatial resolution on the phosphor screen corresponded actually to a 280 μm resolution on the target surface. Note that the use of 6 μm channel MCP would lower the spatial resolution to 70 μm. A major advantage of MCP comes from their lack of sensitivity to visible light. In the present experiment, MCP was protected from plasma VUV emission by a 1 μm polypropylene foil (see Fig. 3). In the case of X-ray spectra in the 8 Å wavelength range, an additional 7 μm Be-foil filter was placed to cut the emission from the first reflection order of the mica crystal. For obtaining K_α spectra of Ca and Cu in the spectral range $\lambda < 3.5$ Å, an additional 90 μm Be filter was placed to cut I–III orders of the crystal reflection.

4. Experimental results

As mentioned above, the spectrometer was tested in the FSSR-1D configuration (see Fig. 1). The main idea of the test experiments was to demonstrate the high tunability of the spectrometer. Once the spectrometer was aligned, due to the unique possibility of the mica crystal to reflect in different diffraction orders, it was possible to record spectra in a wide spectral range (1.5–17.5 Å) with simultaneously good spectral and spatial resolutions.

Actually, the large size of our crystal allows to record spectra over wide wavelength ranges: 15.2–17.5 Å (near resonance line of He-like ion of Fluorine) in the first diffraction order of the mica crystal, 7.6–8.75 Å (spectra between He_α and K_α lines of Al and between Rydberg lines of Ne-like Cu) in the 2nd order, 3.04–3.5 Å (spectra around K_α lines of Ca) in the 5th order and 1.38–1.59 Å (spectra around K_α lines of Cu) in the 11th order of reflection. We did not do test experiments for other mica crystal reflection orders, but in principle, with the same alignment we could obtain spectra in the following spectral range: 5.07–5.83 Å for 3rd order, 3.8–4.4 Å for 4th order, 2.17–2.5 Å for 7th order, 1.9–2.19 Å for 8th order, 1.27–1.46 Å for 12th order, 1.17–1.35 Å for 13th order (see Fig. 4). This figure underlines the high tunability of designed spectrometer. In Figs. 5–9, X-ray spectra from F, Al, Ca and Cu femtosecond laser-produced plasmas are presented. By looking at X-ray images and traces, one can see that we achieved good spectral and spatial resolutions for all investigated targets and for the whole spectral range 1.5–17.5 Å. High spectral resolution is demonstrated in Fig. 5 where complex satellite structures of Li-like ions of Al near the resonance He_α line are resolved. The same structure is also resolved in the 17 Å spectral range near the resonance He_α line of F VIII (see Figs. 7 and 8). In Fig. 9 one can see the resolved components of the $K_{\alpha 1}$ and $K_{\alpha 2}$ lines of Cu.

One can also observe in Figs. 5–9 that a good spatial resolution was obtained in the plane perpendicular to the spectral resolution direction. Fig. 10 summarizes data on the spatial size of the He_α and K_α line emission zones of Al in the X-direction on the surface of the target. We observe the decrease of the size of the K_α line emission zone with decreasing laser intensity on the target surface. The laser intensity was decreased by increasing the focal spot size. In Fig. 5, one can observe important differences in the

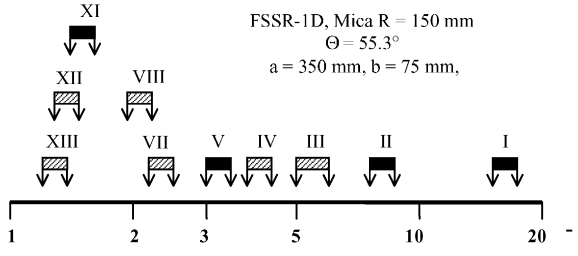

Fig. 4. Spectral ranges, covered simultaneously by a FSSR-1D spectrometer with a spherical mica crystal (the linear size of the crystal in the spectral dispersion direction 50 mm, the radius of crystal curvature is $R = 150$ mm). I, II, III … —mica crystal reflection orders. Reflection orders (I, II, V, XI) tested in present experiments are depicted by black rectangles.

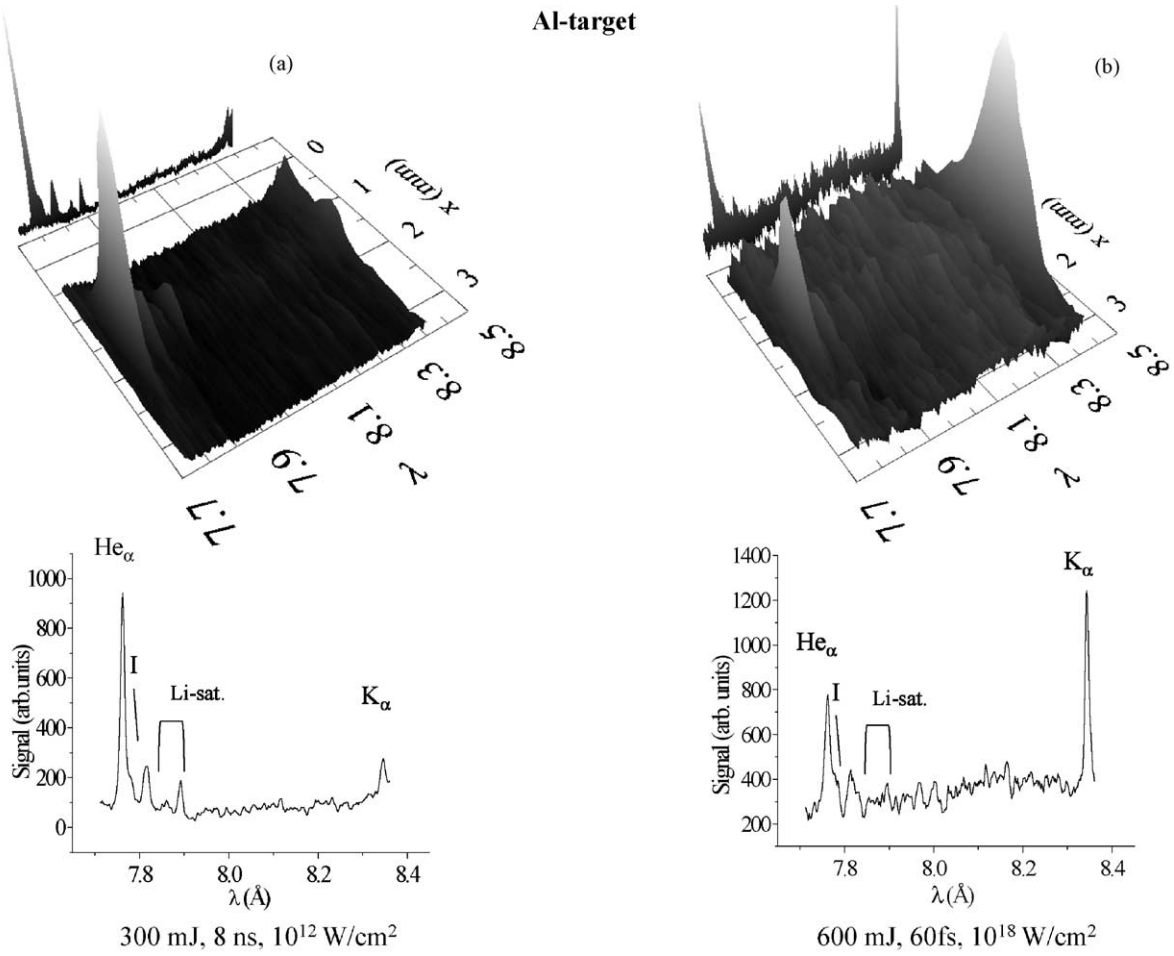

Fig. 5. Space-resolved spectra and lineouts along the highest intensity of He_α line of Al XII obtained by irradiating solid Al targets with Ti : Sa laser pulses such as: (a) 300 mJ, 8 ns, 10^{12} W/cm^2, (b) 600 mJ, 60 fs, 10^{18} W/cm^2. The mica crystal was used in the second-order of diffraction.

relative intensity and in the size of the emission zone of the He_α and K_α lines between nano- and femtosecond laser-produced Al plasmas. These images are being analyzed now and results will be published later on.

Thanks to the high luminosity of the FSSR-1D spectrometer and the high sensitivity of the MCP assembly, spectra of F and Al were recorded on a single laser shot. The intensity of the He_α line of F VIII was even saturated on a single laser shot if the voltage applied on the MCP was greater than 1250 V. Because of an efficient hot electron production in the interaction of femtosecond laser pulses with solid targets, a strong hard X-ray

Fig. 6. Space-resolved spectra and lineouts along the highest intensity of He_α line of Al XII obtained by irradiating solid Al targets with Ti : Sa laser pulses of 600 mJ energy, 60 fs pulse duration and a laser intensity of 10^{18} W/cm^2 (a), 1.5×10^{16} W/cm^2 (b), 2.5×10^{15} W/cm^2 (c) and 10^{15} W/cm^2 (d). Decreasing of laser intensity was achieved by increasing the size of laser focal spot without changing other laser parameters. The mica crystal was used in the second-order of diffraction.

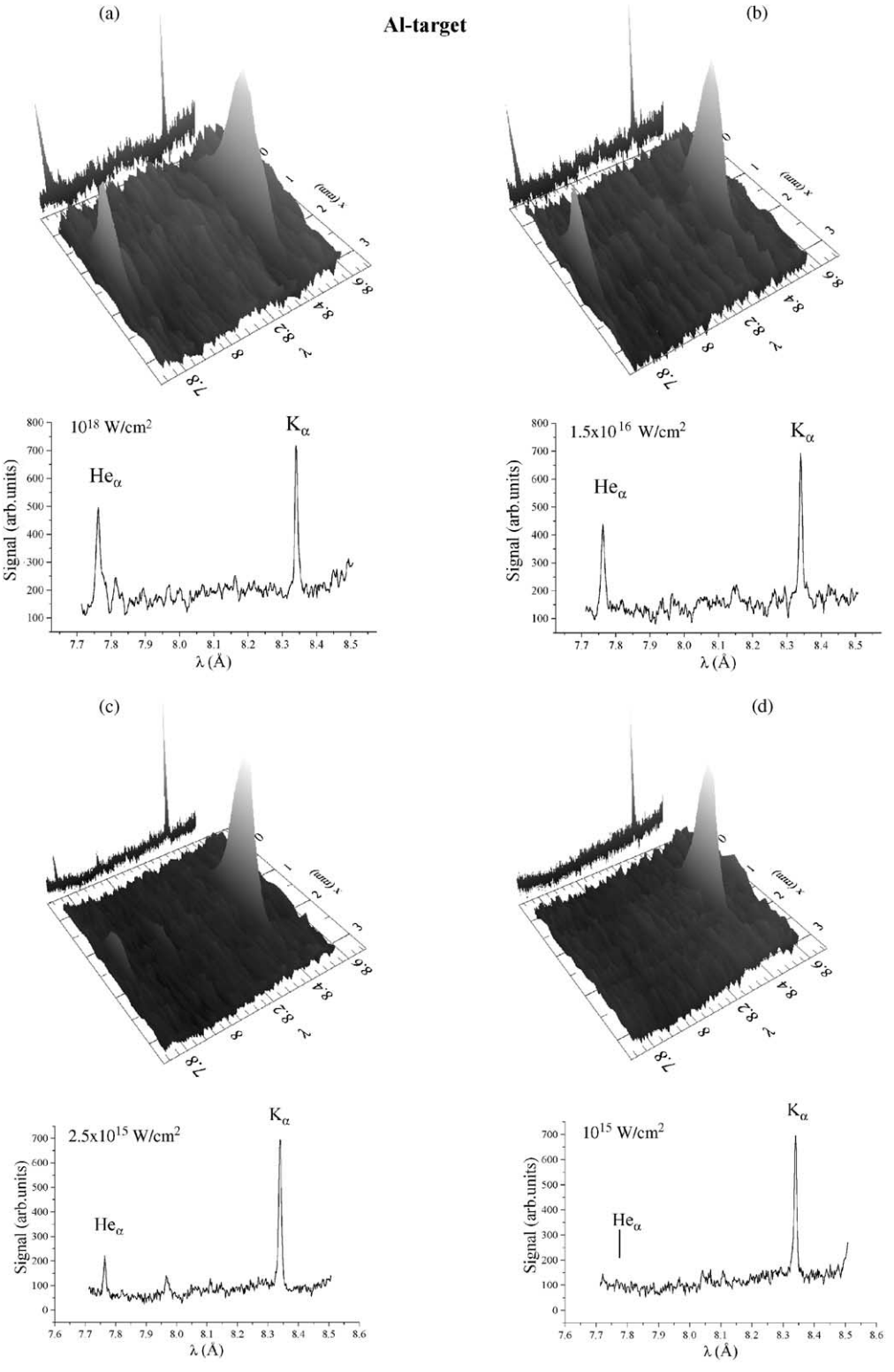
Al-target
(a)
(b)
(c)
(d)
x (mm)
10^{18} W/cm^2
1.5×10^{16} W/cm^2
2.5×10^{15} W/cm^2
10^{15} W/cm^2
K_α
He_α
Signal (arb.units)
λ (Å)

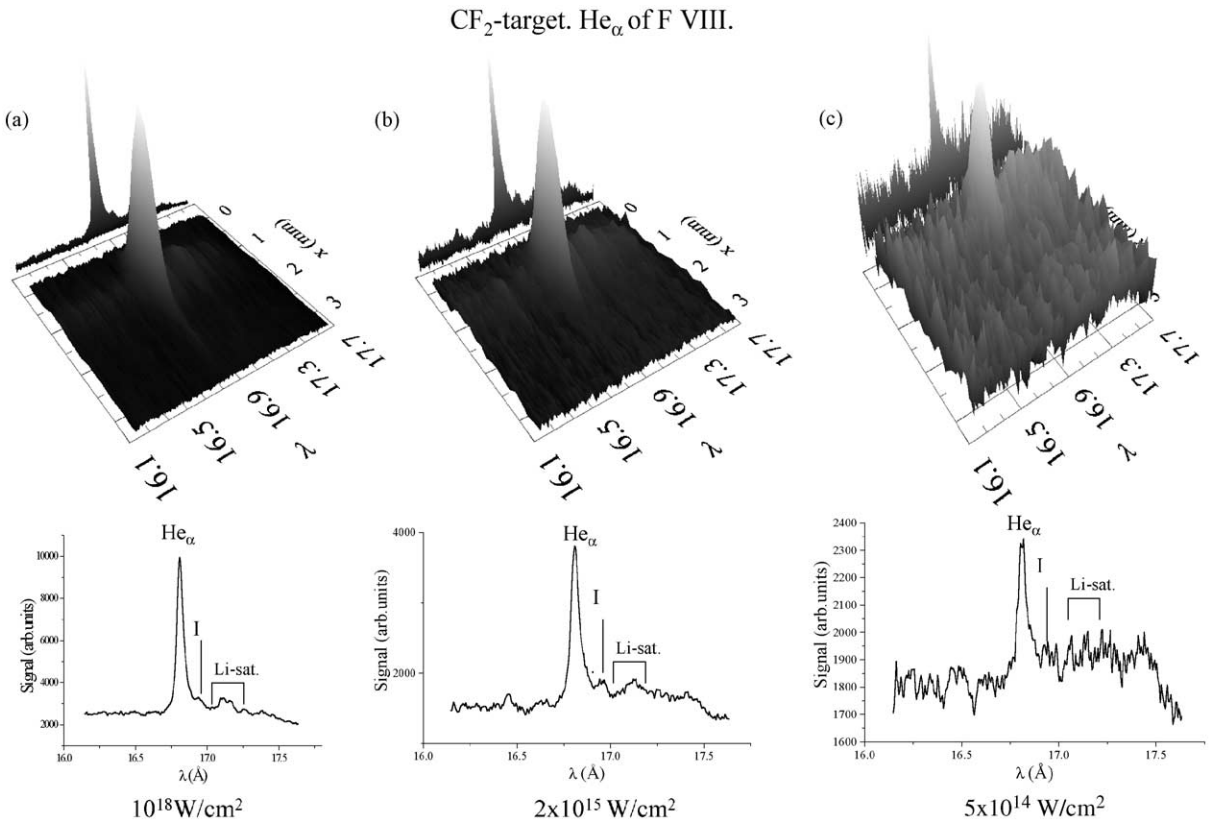

Fig. 7. Space-resolved spectra and lineouts along the highest intensity of He_α line of F VIII obtained by irradiating solid $(CF_2)_n$ targets with Ti : Sa laser pulses with 600 mJ energy, 60 fs pulse duration and a laser intensity of 10^{18} W/cm^2 (a), 2×10^{15} W/cm^2 (b) and 5×10^{14} W/cm^2 (c). The mica crystal was used in the first-order of diffraction.

emission does exist and was responsible here for a background on the MCP. Therefore, it was necessary to sum up over several shots in all above mentioned experiments in order to increase the signal-to-noise ratio. Nevertheless, due to the high sensitivity of the spectrometer it was necessary to do only 10–50 laser shots to obtain contrasted space-resolved spectra. The high sensitivity of the system is also demonstrated from experiments with nanosecond laser pulses interacting with solid Al (Fig. 5a). We obtained spectra with a good quality between the He_α and K_α lines on a single shot for a weak laser intensity ($I \approx 10^{12}$ W/cm^2). In the case of interaction with femtosecond pulses, the high sensitivity of the device allowed us to receive spectrally resolved images of the He_α and K_α lines of Al for laser intensity as low as 10^{15} W/cm^2 (see Fig. 6d). Other spectra near the He_α line of F VIII was obtained for 5×10^{14} W/cm^2 laser intensity (see Fig. 7c). Another illustration of the high efficiency of our spectrometer is demonstrated by the fact that we were able to obtain spectra of Rydberg resonance lines of Ne-like Cu XX, which have not been observed up to now in femtosecond laser-produced plasma experiments (see Fig. 9) because of their weak emission.

Finally, it is worthnoting that our experimental spectra were obtained with spatial resolution while, for typical X-ray spectrometers with flat or cylindrically bent crystals, spatial resolution is absent. We would like once more to underline another important advantage of our spectrometer:

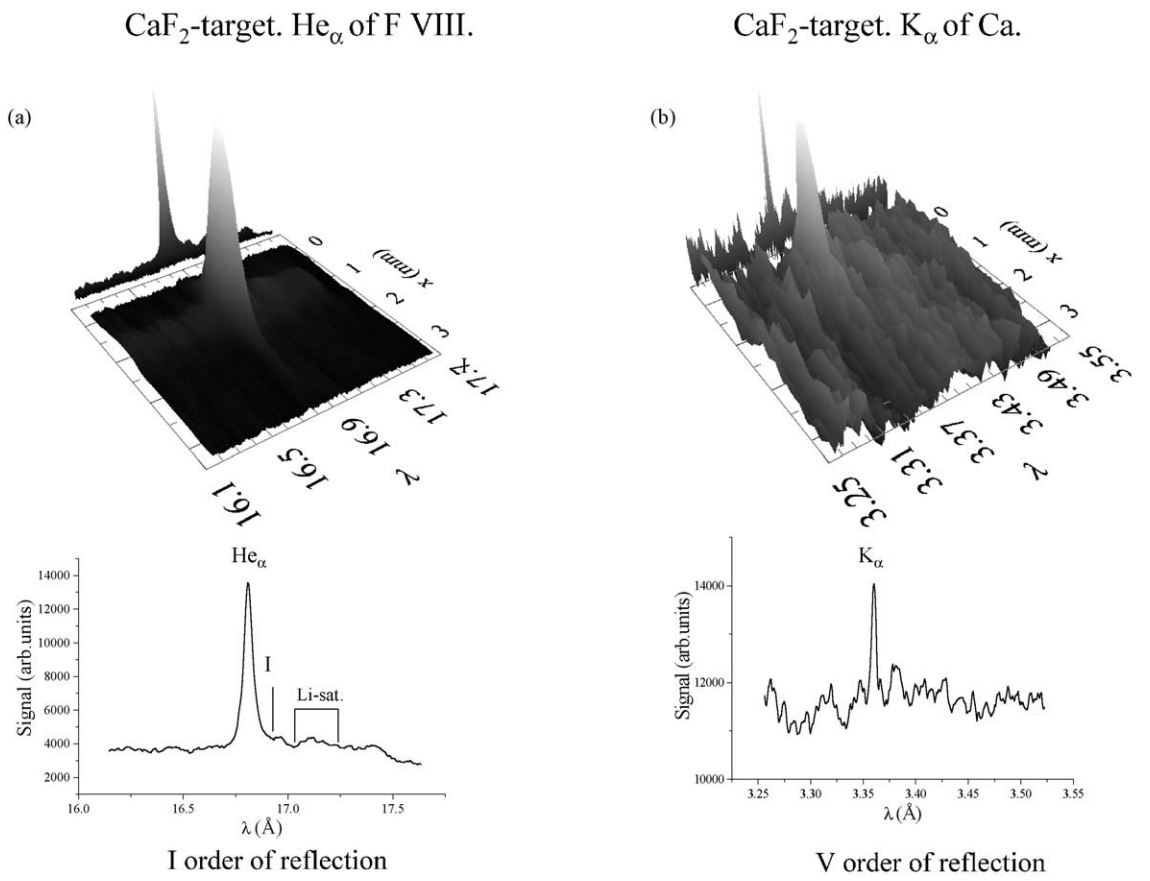

Fig. 8. Space-resolved spectra and lineouts along the highest intensity of He_α line of F VIII (a) and K_α line of Ca (b) obtained by irradiation of solid CaF_2 targets with Ti : Sa laser pulses, 600 mJ energy, 60 fs pulse duration and 10^{18} W/cm^2 laser intensity. The mica crystal was used in the first order of diffraction to obtain spectra of Fluorine and in the 5th order for registration spectra of Ca.

its high spectral tunability. All the spectra reported here, obtained in the 1.38–17.5 Å wavelength range, were recorded with only one spectrometer alignment.

5. Conclusion

We have successfully designed and tested a high-sensitive, portable, tunable, imaging X-ray spectrometer based on a spherically bent, large aperture mica crystal with a small radius of curvature and a MCP assembly as a detector. The advantages of this spectrometer are:

(1) A high luminosity due to the large open aperture, small radius of curvature and the focusing properties of the spherically bent crystals on the one hand and to the use of MCP assembly as a detector on the other hand.
(2) A small size, which allows to place the spectrometer very close to the X-ray source, in any target chamber.
(3) Good spectral and spatial (perpendicular to the dispersion plane) resolutions, obtained simultaneously.
(4) A wide spectral range covered (between 1.2 and 19.6 Å) using multiple diffraction orders of mica crystals.
(5) A good versatility, which allows to record spectra from different targets with only one alignment set-up.

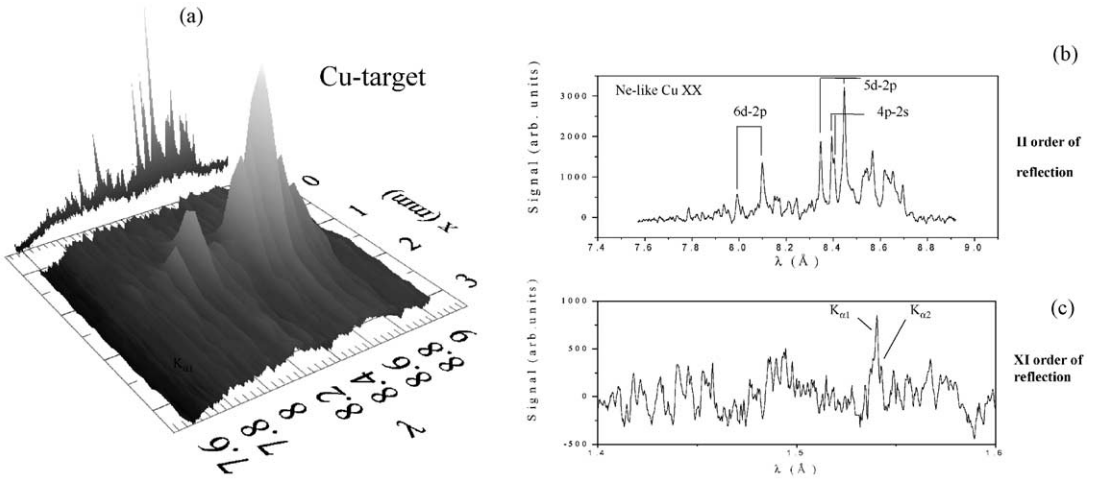

Fig. 9. Space-resolved spectrum (a) and lineouts (b) along the highest intensities of resonance Rydberg lines of Ne-like ions of Cu XX and $K_{\alpha 1,2}$ lines of Cu (c), obtained by irradiating Cu targets with Ti : Sa laser pulses of 600 mJ energy, 60 fs pulse duration and 10^{18} W/cm^2 laser intensity. The mica crystal was used in the second-order of diffraction to obtain Rydberg lines spectra of Ne-like Cu and in the 11th order for Cu $K_{\alpha 1,2}$ lines spectra.

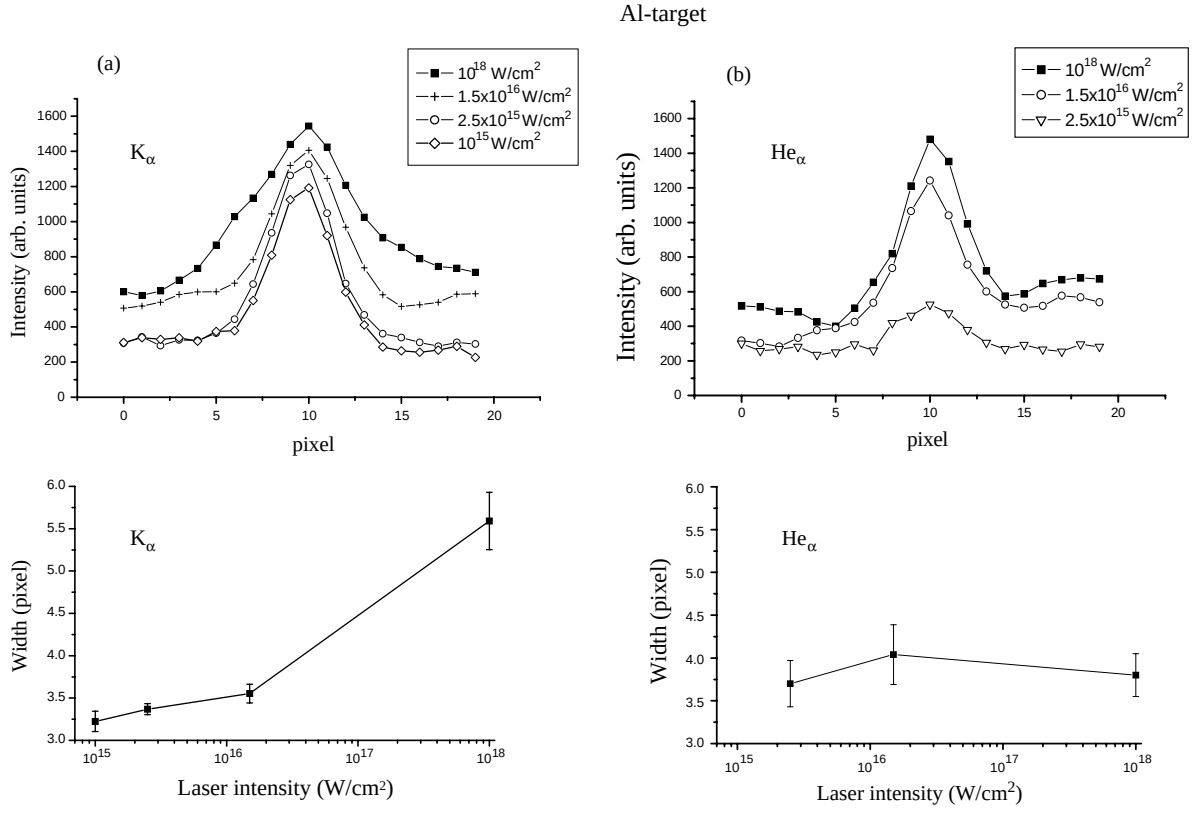

Fig. 10. Spatial size of the emission zone of the Al K_α (a) and He_α (b) lines as a function of the laser intensity.

(6) A real time acquisition of X-ray space-resolved spectra due to the coupling of the spectrometer with the MCP assembly and the CCD camera linked to a computer.

References

[1] O. Ellegaard, et al. (Eds.), Proceedings of the 18th International Conference on atomic Collisions in Solids, Odense, Denmark, 1999. Nucl. Instr. and Meth. B 164–165 (2000).
[2] W. Möller, et al. (Eds.), Proceedings of the 14th International Conference on Ion Beam Analysis/Sixth European Conference on Accelerators in Applied Research and Technology, Dresden, Germany, 1999. Nucl. Instr. and Meth. B 161–163 (2000).
[3] K.G. Malmqvist (Ed.), Proceedings of the Eighth International Conference on Particle Induced X-ray Emission and its Analytical Applications, Lund, Sweden, 1998. Nucl. Instr. and Meth. B 150 (1–4) (1999).
[4] R.W. Lee (Ed.), Radiative properties of hot dense matter IV (Special Issue), J. Quant. Spectrosc. Radiat. Transfer 65 (1–3) (2000).
[5] A.Ya. Faenov, S.A. Pikuz, A.I. Erko, B.A. Bryunetkin, V.M. Dyakin, G.V. Ivanenkov, A.R. Mingaleev, T.A. Pikuz, V.M. Romanova, T.A. Shelkovenko, Phys. Scripta 50 (1994) 333.
[6] T.A. Pikuz, A.Ya. Faenov, S.A. Pikuz, V.M. Romanova, T.A. Shelkovenko, J. X-ray Sci. Technol. 5 (1995) 323.
[7] I.Yu. Skobelev, A.Ya. Faenov, B.A. Bryunetkin, V.M. Dyakin, T.A. Pikuz, S.A. Pikuz, T.A. Shelkovenko, V.M. Romanova, A.R. Mingaleev, JETP 81 (1995) 692.
[8] B.K.F. Young, et al., Rev. Sci. Instr. 69 (1998) 4049.
[9] N. Nakamura, A.Ya. Faenov, T.A. Pikuz, E. Nojikawa, H. Shiraishi, F.J. Curell, S. Ohtani, Rev. Sci. Instr. 70 (1999) 1658.
[10] A. I. Magunov, A. Ya. Faenov, T. A. Pikuz, I. Yu. Skobelev, Ray-tracing code for focusing spectrometers with spatial resolution (FSSR-1, 2D), MISDC, VNIIFTRI, 1997.
[11] G.W. Fraser, Nucl. Instr. and Meth. 195 (1982) 523.
[12] T.A. Pikuz, A.Ya. Faenov, E. Förster, J. Wolf, O. Wehrhan, J. Heinisch, G. Hoelzer, M. Vollbrecht, S.A. Pikuz, V.M. Romanova, T.A. Shelkovenko, Proc. SPIE-95. 2515 (1995) 468.
[13] G. Höelzer, O. Wehrhan, J. Heinisch, E. Förster, T.A. Pikuz, A.Ya. Faenov, S.A. Pikuz, V.M. Romanova, T.A. Shelkovenko, Phys. Scripta 57 (1998) 301.
[14] B.K.F. Young, et al., Rev. Sci. Instr. 69 (1998) 4049.